Electronic transport through single-molecule oligophenyl-diethynyl junctions with direct gold - carbon bonds formed at low temperature

Gautam Mitra[1], Vincent Delmas[2], Hassan Al Sabea[2], Lucie Norel[2], Olivier Galangau[2], Stéphane Rigaut[2], Jérôme Cornil[3], Karine Costuas[2], Elke Scheer[1]

[1] University of Konstanz, Department of Physics, 78457 Konstanz, Germany
[2] University of Rennes, CNRS, ISCR (Institut des Sciences Chimiques de Rennes) – UMR 6226, F-35000 Rennes, France
[3] University of Mons, Laboratory for Chemistry of Novel Materials, Department of Chemistry, Place du Parc 20, B-7000 Mons, Belgium

Abstract

We report on the first systematic transport study of alkynyl-ended oligophenyl-diethynyl (OPA) single-molecule junctions with direct Au - C contacts formed at low temperature using the mechanically controlled break junction technique. Through quantitative statistical analysis of opening traces, conductance histograms and DFT analysis, we identified different types of junctions, classified by their conductance and stretching behavior, for OPA molecules between Au electrodes with two to four phenyl rings. We performed inelastic electron tunneling spectroscopy and observed the excitation of Au-C vibrational modes confirming the Au-C bond formation and compared the stability of molecule junctions upon mechanical stretching. Our findings reveal the huge potential for future functional molecule transport studies at low temperature using alkynyl endgroups.

1 Introduction

Charge transport studies through different functional molecules with high stability and robustness are key for the development of molecular electronics.[1, 2] Usually, the molecule is chemically functionalized with an endgroup responsible for bridging between electrodes and forming single-molecule junctions.[3, 4, 5, 6] Endgroups with sufficiently strong bonding, long stretching distance and electronically transparent nature are ideal candidates for molecular electronic devices. To study the in-depth electronic and magnetic transport properties of different functional molecules, the ability to form single-molecule junctions which are stable and robust at low temperature and in vacuum are also of particular interest for choosing endgroups. Thiols (-SH).[8, 11], amines (-NH_2)[7, 9, 10], cyanides (-CN) [11], pyridines [4, 12] are among the most commonly used endgroups for their coupling strengths and known contact geometries. Recently, there is surging interest on the line of establishing direct gold carbon (Au - C) covalent bonds to achieve more robust and highly conducting molecular junctions.[13, 14, 15, 16, 17, 18, 19, 20] Initial studies with Au - C bonded single-molecule junctions were observed by Venkataraman's group on methylene terminated oligophenyls and polymethylene chains which shows near resonant transport and enhanced conductance compared to other endgroups.[13] Hong et al. characterized the (oligo)-phenylene-ethynylene (OPE) derivatives using Raman scattering[18] and Arasu et al. proposed bipodal platforms based on biphenylene with two Au - C bonds which show very stable and electronically transparent properties of Au - C anchoring scheme.[19] The direct Au - C bond formation can be experimentally realized using highly toxic $SnMe_3$ linkers, which cleave off on contact with Au electrodes [13, 14, 20] and also with in situ cleavage of trimethylsilyl group attached to alkynyl moiety using tetrabutylammonium fluoride.[18] Recently, another binding mechanism based on alkynyls forming direct Au - C bonds without the need for any precursors was reported.[21] So far, all these experiments have been performed in

solution at room temperature. Characterizations with photoemission spectroscopy have shown that it is also possible to form Au - C bonds in ultrahigh vacuum conditions.[22] However, to the best of our knowledge, a detailed characterization of single-molecule junctions with direct Au - C covalent σ bonds at low temperature under vacuum conditions has not been realized so far. This would, however, be important to establish long-lived junctions, also with functional entities included which allow to study their transport properties in detail due to low thermal noise and sub angstrom level mechanical manipulation of molecule junctions.

Here we report the first systematic study of single-molecule junctions with Au - C anchoring units at low temperature, down to 4.2 K. We have used oligophenyl-diethynyl molecules with alkynyl endgroups which we denote as OPAn ($n = 2, 3, 4$); n represents the number of phenyl units as shown in Figure 1. Since these have been already reported to form molecule junctions at ambient conditions without any need of precursors,[21] they represent an ideal platform for a comparison of conductance and for further characterizations. We find that the resulting molecular junctions are highly robust and reproducible over several weeks at 4.2 K. Our mechanically controlled break junction (MCBJ) setup at low temperature offers the stability to carry out advanced experiments like inelastic electron tunneling spectroscopy (IETS). Although IETS observations are known for several other anchoring groups,[32, 36, 37] an experimental characterization of vibrational modes from single-molecule junctions with Au - C linkers is still unknown. Thus, with the help of IETS at low temperature, we confirmed the excitation of the Au - C vibron modes, as a signature for successful Au - C bond formation and able to give an insight into the junction characteristics upon stretching by using the variation of different vibrational modes. In order to get a theoretical insight into the understanding of the IET spectra, quantum - chemical calculations at the density functional theory (DFT) for the isolated molecules and tight-binding density functional theory (DFTB) level for both isolated and gold-coordinated molecules were also performed (see computational details in SI).

2 Experimental and Characterization Measurements

We prepared 5 mM of OPAn molecule solutions using dichloromethane (DCM) as solvent under a nitrogen atmosphere. We observed that the yield of molecular junctions formed with lower concentrations is very small, see Figure S1 in the SI. These freshly prepared molecular solutions were drop-casted at room temperature on a free-standing Au bridge on a bronze substrate fabricated using electron beam lithography and dry etching techniques.[23, 24, 25] When brought into contact with Au electrodes, the hydrogen atoms at the outer ends of the molecule cleave off and direct Au - C bond formation can take place.[26] This method avoids any need for additional precursors leaving toxic groups in the solution. Single-molecule junctions are formed using the mechanically controllable break junction (MCBJ) technique, a schematic of which is shown in Figure 1. We dried the samples in nitrogen flow, cooled them down and broke the Au wires in cryogenic vacuum at low temperature by bending the substrate in the MCBJ mechanics. Electrical transport measurements were carried out at 4.2 K. Because of the purely mechanical drive, the opening speed is limited to about one opening trace per≈ 10 min, which then limits the maximum number of opening traces that can be recorded in a reasonable time span to a few hundreds. First, we open and close the samples to form Au contacts and molecule junctions repeatedly. The conductance G is measured using the current and voltage ratio at fixed bias voltage across the junctions. The evolution of G during this process is evaluated as a function of displacement between the Au electrodes. From these data, we construct so-called one-dimensional (1D) conductance histograms using logarithmic binning of these opening conductance traces.

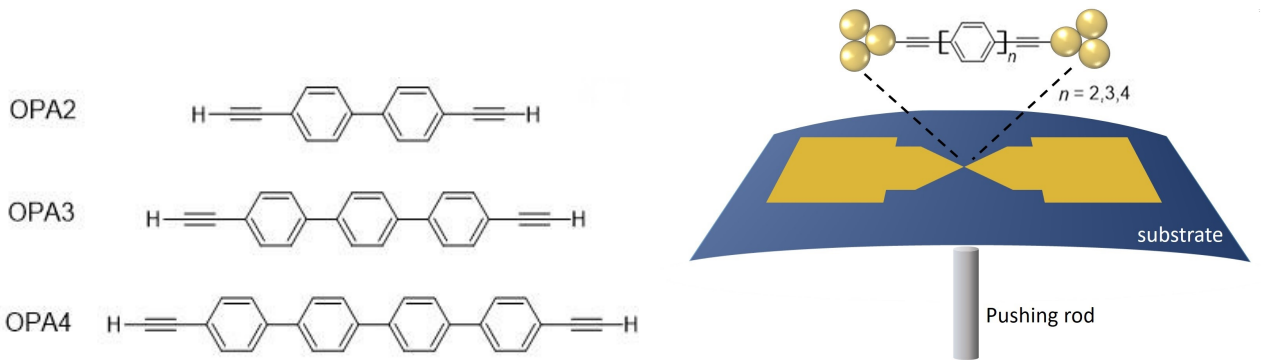

Figure 1: Molecules used for the current study are shown on the left and the mechanically controlled break junction (MCBJ) schematics is shown on the right.

Figure 2 shows typical individual traces obtained for each species under study. The noise floor of the measurement unit is below 10^{-6} G_0 with the conductance quantum $G_0 = 2e^2/h$. Au single-atom contacts form on every opening trace confirmed by the plateau formation at 1 G_0. After breaking the Au - Au contacts, we observed conductance plateaus at different G for the different molecules. These plateaus are attributed to molecular junctions formed between the sharp Au electrodes with $\mathrm{R-C\equiv C-H}$ as endgroup where R denotes the rest of the OPAn chain. The length of plateaus increases with molecular length, although there are some exceptions which we will discuss in the next paragraph. Upon further stretching of the junctions, their conductance finally drops to the noise level signaling the breaking of the junction, then forming a vacuum tunneling contact. The molecular junctions are robust over time and reproducible even after one week of measurement. The nominal length of fully stretched Au-OPAn-Au junctions corresponds to 1.2, 1.6 and 2.1 nm, for $n = 2, 3$, and 4, respectively.[21] The uncertainty in the determination of the plateau length in our MCBJ molecular junctions is estimated to be in the order of 30%. We therefore mainly discuss relative length variations between the molecules. In addition, we study the IET spectra of individual junctions by using a lock-in technique in a bias range from -300 to 300 mV and an AC modulation voltage of 3 mV. For more details, see SI.

3 Results and Analysis

Figure 2 shows the examples of typical opening traces and corresponding 1D histograms obtained from 300 - 500 traces measured at 100 mV bias voltage applied to OPAn molecules at low temperature. We have labeled maxima with higher conductance as HC and lower conductance as LC in the histograms. These histograms are constructed without any data selection.

The histogram of OPA2 has one shoulder (HC) around 2×10^{-4} G_0 and another (LC) around 3×10^{-5} G_0 in the 1D histogram (Figure 2b). The majority of the opening traces in OPA2 has flat plateaus near 10^{-4} G_0 with a length of 0.2 - 0.5 nm. We have also observed slanted plateaus of length up to 1.5 nm starting at conductance values slightly higher than 10^{-4} G_0 and decreasing conductance upon stretching before finally breaking to the noise level. We are attributing the latter to the presence of dimerized OPA2 systems in the junctions (OPA2-OPA2) resulting of alkynes homocoupling and the possibility of having a part of the molecule lying over the electrode surfaces as sometimes observed for long molecules.[27, 44, 45]

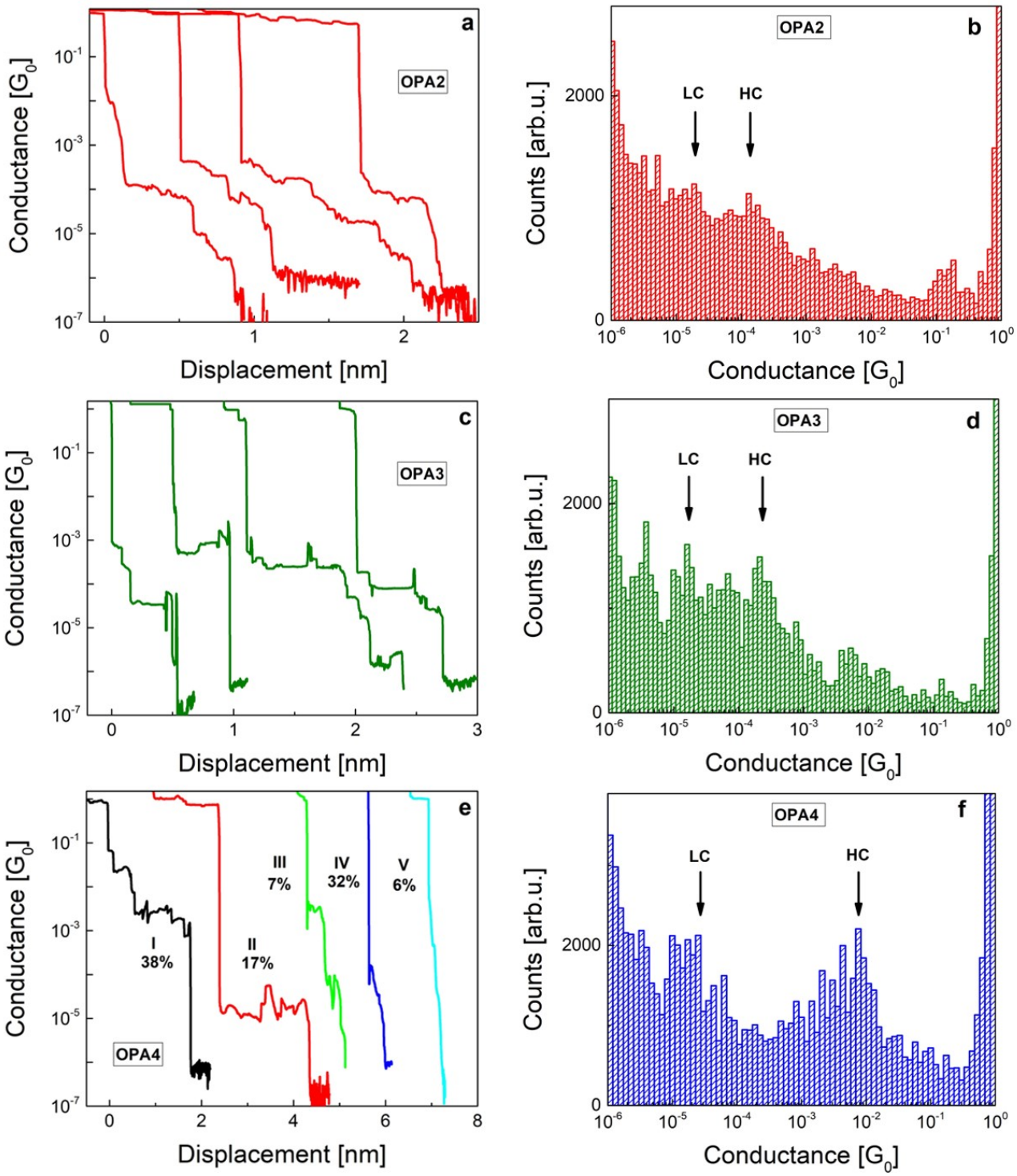

Figure 2: Examples of opening traces with molecular plateaus and 1D histograms observed from OPA2 (a,b), OPA3 (c,d) and OPA4 (e,f) respectively measured at low temperature with an applied bias voltage of 100 mV. Displacement is measured as the inter electrode distance upon stretching the junction. Maxima of histograms are labeled as HC and LC for higher and lower conductance respectively. The probability of each type of traces observed from OPA4 molecule is also shown

.

OPA3 shows pronounced flat plateaus between 10^{-3} G_0 and 10^{-4} G_0 of length 0.6 to 1 nm as shown in Figure 2c, corresponding to a single OPA3 molecule bridged between Au tips. The conductance of OPA3 molecular plateaus is slightly higher than that of OPA2 which is in

agreement with the reported room temperature studies.[21] The OPA3 histogram has a maximum near 3.5×10^{-4} G_0 (HC) and the probability of stretched junctions extends until 10^{-5} G_0 (LC) (Figure 2d). The molecular yield for OPA3 is 38%. Beside the two maxima labeled as HC and LC, the histogram of OPA3 shows additional peaks at very low conductance. We attribute these to different junction binding configurations and also the presence of molecular chains of OPA3 units. This is also evident from the traces due to the long plateau length upon stretching towards lower conductance. The probability of these traces is much higher for OPA3 compared to OPA2 and OPA4 leading to a much broader histogram peak.

OPA4 exhibits five different kinds of molecular traces in contrast to OPA2 and OPA3. Figure 2e shows the frequently observed traces for OPA4 which are classified based on observed conductance, plateau length and their probability of formation. We observed long flat plateaus up to 1.5 nm length and conductance between 10^{-2} G_0 and 10^{-3} G_0 (Type I) and further long plateaus of length up to 2 nm with a conductance around 10^{-5} G_0 (Type II). There were also traces (Type III) which include flat plateaus at higher (10^{-3} G_0) and lower conductance (10^{-5} G_0) with a total plateau length around 0.5 nm. In addition to that, some opening traces include slanted plateaus starting at lower conductance (10^{-4} G_0) and at higher conductance (10^{-2} G_0), which we refer to as Type IV and Type V traces, respectively. These traces have very short lengths of less than 0.5 nm. To further confirm the presence of these traces, we have carried out OPA4 measurement on multiple samples and made a statistical evaluation of the traces obtained. We analyzed 515 opening traces for OPA4 and the yield of traces revealing molecular behavior was 32%. From these, we have analyzed the percentage of molecular traces belonging to each category. The majority of traces falls into Type I with 38% probability. The next category of long plateaus is Type II with 17% abundance agrees with the molecule junction conductance found in previous studies at ambient conditions.[21] Therefore, we suspect molecule junctions aligned in parallel or $\pi - \pi$ stacking of molecules give rise to Type I traces.[33] Type IV traces signal junctions chemically bonded to one electrode only and are found in 32% of molecular traces. Type III and Type V were only observed in 7% and 6% of traces, respectively, indicating some molecular junctions which are not well connected to the electrodes and breaks apart easily upon stretching, resulting short plateau length. A bar diagram comparing these results is shown in Figure S2 in SI. Summarizing this as a 1D histogram in Figure 2f, we observed a maximum at 7.5×10^{-3} G_0 (HC) and a second maximum at 3×10^{-5} G_0 (LC). We have also looked at the evolution of the relative abundance of the various types with time and found no particular trend. This indicates that the different types of traces are not caused by training or aging effects due to the mechanical deformation, but reveal different types of junction formation.

We observed an increase in the HC conductance as the number of phenyl groups increases which is in contradiction with the usual trend of exponential decay of conductance with molecular length for hydrocarbon molecules with off-resonant transport.[28] However, a non-exponential, but still decreasing conductance with length was previously found for OPAn junctions at room temperature.[21] The authors also noted a pronounced variation of the most probable conductance on the concentration of the molecular solution, suggesting that in their study, the formation of molecule junctions connected in parallel might play a role. In our case, the higher concentration of molecular solution used may have affected this behavior especially in the case of OPA4 although the junction formation was minimal at low temperature for lower concentration (see figure S1 in the SI). We have calculated the transmission spectra of Au - OPA_n - Au junctions at the DFT + NEGF level (computational details in SI). For the chemical anchoring, the terminal carbon has been positioned in top coordination mode on the gold (111) electrode surface (Figure S7). The corresponding transmission spectra are given in Figure S8. The calculated conductance (G) are about 2 orders of magnitude higher than the experimental

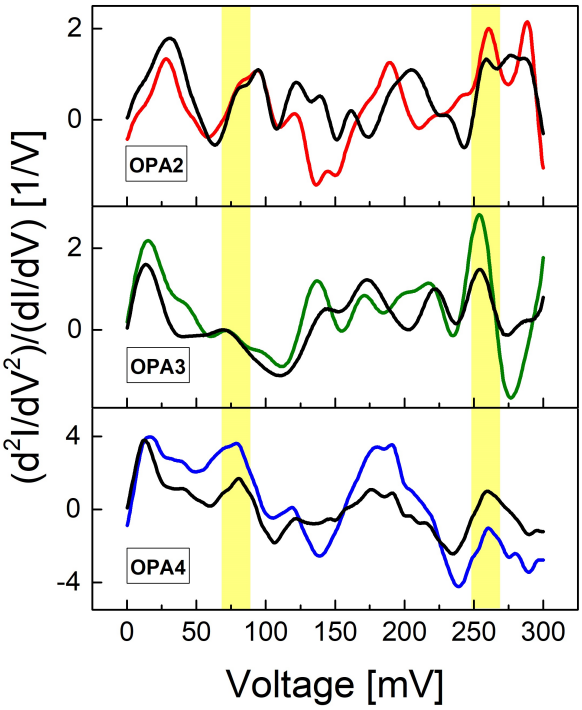

Figure 3: Comparison of experimental inelastic electron tunneling spectra (IETS) for OPA2, OPA3 and OPA4 are shown with red, green and blue curves, respectively. Symmetrized IETS spectra calculated for each molecular junction as $y = [f(x) - f(-x)]/2$ are shown as black lines in each figure. The yellow regions indicate the typical energies of Au - C vibrons (in 60 - 75 mV) and of the C $\equiv$ C stretching mode (250 - 275 mV).

high conductance peak for the symmetric OPA2, OPA3 and OPA4 junctions as expected for this level of theory for this most stable coordination[40, 41]. In order to evaluate the homo coupling that has been observed experimentally in some studies,[44, 45] the OPA2-OPA2 junction was also added to the series and turns out to have a conductance value intermediate between OPA3 and OPA4. Thus the possibilty of dimerization resulting of alkyne homocoupling cannot be excluded. Such dimerization is surely occurring for OPA3 and for OPA4, but the resulting lengths of the dimeric systems especially for OPA4 diminish their probability to form molecular junctions via the present MCBJ method.

We provide further evidence for the Au - C linked molecular junctions at low temperature by analyzing the most prominent vibrational modes found in these molecular devices. The IET spectrum is defined as (d^2I/dV^2) normalized with the differential conductance dI/dV to be able to compare spectra gathered from junctions with different conductance. We measured the spectra over a fixed bias range of -300 mV to 300 mV and symmetrized using the simple formula $y = [f(x) - f(-x)]/2$, to suppress contributions that might arise from conductance fluctuations or other phenomena, since the IET spectrum is expected to be symmetric. We directly measured IETS for OPA3 and OPA4 junctions with conductance around 10^{-3} G_0 using a lock-in amplifier. In the case of OPA2, the IET spectrum was numerically derived from the dI/dV curve of a HC junction, due to the limited lock-in sensitivity in this conductance range (see SI for comparison with numerical derivative and lock-in measurement).

Figure 3 compares examples of experimental and symmetrized IETS from 0 - 300 mV from

a single junction for each OPAn molecule. Previous studies of surface enhanced Raman characterizations on molecular systems involving Au - C covalent bonds determined the Au - C stretch near 46 - 52 mV. [18, 38] Later, Giuseppe et al. using first principle simulations of IETS in metal-molecule junctions, found a signature of the Au - C stretch vibration mode near 60-70 mV.[29] Our OPAn devices show characteristic bands around 60-75 mV, which we attribute to the longitudinal vibrations of the Au - C bond. The C $\equiv$ C stretching mode is also observed in all our molecular junctions at 250 - 270 mV [18] as shown in Figure 3. In addition to that, we observed the typical Au phonon mode near 10 - 20 mV,[30] ring breathing near 140-160 mV and typical ring vibrations at 190-220 mV in all molecules.[31, 34, 35] We have carried out the IETS measurements on multiple HC junctions and the phonon modes are found to be prevalent even after averaging over all the measured spectra, see Figure S4 in the SI. This strong signature of Au - C and C $\equiv$ C vibration modes provides a direct evidence of stable Au - C linked molecular junctions at low temperature. Due to the limited resolution of the IETS at low conductance, we were only able to study the IETS in the HC regime of the OPAn junctions.

In order to get a detailed understanding of IETS and the junction configurations, we have also carried out DFT simulations of the density of vibrational states of OPA2 and OPA3 together with the simulated infrared and Raman spectra (Figure S11). The vibrational modes are in good agreement with the available experimental data (calculated C $\equiv$ C stretching mode = 265 meV for the two compounds, IR experimental C $\equiv$ C frequency = 261 meV for OPA2 and OPA3)[43]. DFT phonon calculations of the entire molecular junctions could not be performed because of excessive memory requirements. DFTB calculations were thus performed. The C $\equiv$ C stretching modes are slightly overestimated compared to DFT ($\approx$ 20 meV) mostly because of the optimized C $\equiv$ C bonds are slightly longer at the DFTB level. Although the overall density of vibrational state spectra is in really good agreement between DFT and DFTB results (Table 1). This supports the validity of the qualitative trends which can be obtained by DFTB. The vibrational study was extended to Au-coordinated molecules by employing a cluster-type model, i.e., by coordinating the terminal carbon atoms to Au_3 clusters. Additionally to a carbon-gold coordination at both ends of the molecule (A), a single coordination to one of the electrodes was also considered (B). Alternative scenarios were considered for OPA2: an arrangement in which the terminal hydrogens do not leave upon binding (C); the same arrangement considering that hydrogen migration occurs to the adjacent carbons (D); a non-symmetrical configuration with case A on one side and case C on the other side (E); single gold-coordination as in case B but considering that the terminal hydrogen would have been removed during the process (F) (Table 1). The geometries of all the arrangements were fully optimized at the DFTB level. The vibrational signature of the Au-C(molecule) binding is calculated in the range 30 - 50 eV for the whole series, a value probably underestimated (due to the cluster-type model) but in line with IETS results, reinforcing the chemical anchoring scheme. It has to be noted that these low-energy vibrational modes are a collective motion of atoms involving gold atoms and most of the carbon atoms of the molecules. The study of the results in Table 1 reveals that the C $\equiv$ C bond vibrational modes are lowered by roughly 10 meV when the terminal carbon is substituted by Au_3 (OPAn-A). The Au_3-C $\equiv$ C vibrational signature is found at roughly 275 meV in this case. The calculated density of vibrational modes of the OPA2-A system reported in Figure S6 reveals that this peak is well-separated from the rest of the vibrational modes (same result for OPA3-A and OPA4-A). The experimental IET spectra for the HC regime junctions show essentially this signature.

Interestingly, the IETS of OPA2 in this region shows at least two peaks (Figure 3). Several scenarios were considered to explain this feature. First, if only one end of the molecule was chemically anchored (case B and F), the calculated vibrational signatures are made of two

Table 1: DFTB calculated energies of the characteristic vibrational modes (meV) and their localization for OPA2, OPA2-OPA2, OPA3 and OPA4 molecules and coordinated to two Au_3 clusters at both ends (A), coordinated to one Au_3 cluster (B). DFT energies are given in parenthesis. (DFT-simulated Raman and IR spectra are given in Figure S5). For OPA2, different scenarios were added (see text).

	Coordination	Molecule Length (nm)	Au - C	C ≡ C	C=C-H
OPA_2	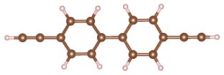	1.46	-	283 (265)	-
OPA_2 -A	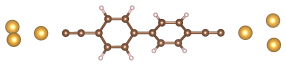	1.24	38	275	-
OPA_2 -B	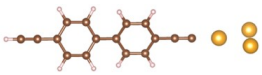	1.35	26	275, 283	-
OPA_2 -C	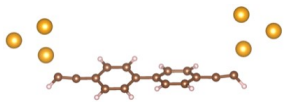	1.39	43	249	-
OPA_2 -D	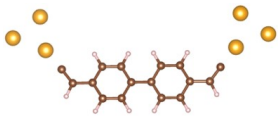	1.16	43	-	220
OPA_2 -E	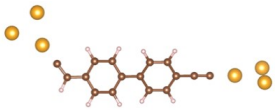	1.21	48	275	219
OPA_2 -F	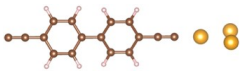	1.25	27	274, 267	-
$(OPA_2)_2$		2.84	-	283, 290	-
$(OPA_2)_2$ -A		3.02	42	275, 290	-
OPA_3	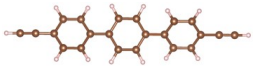	1.90	-	283 (265)	-
OPA_3 -A	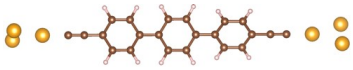	1.68	40	275	-
OPA_3 -B	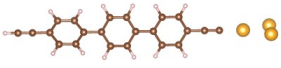	1.78	37.3	275, 283	-
OPA_4	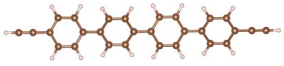	2.32	-	283 (265)	-
OPA_4 -A	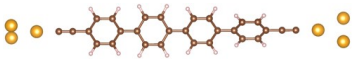	2.11	38	275	-
OPA_4 -B		2.21	36.5	275, 283	-

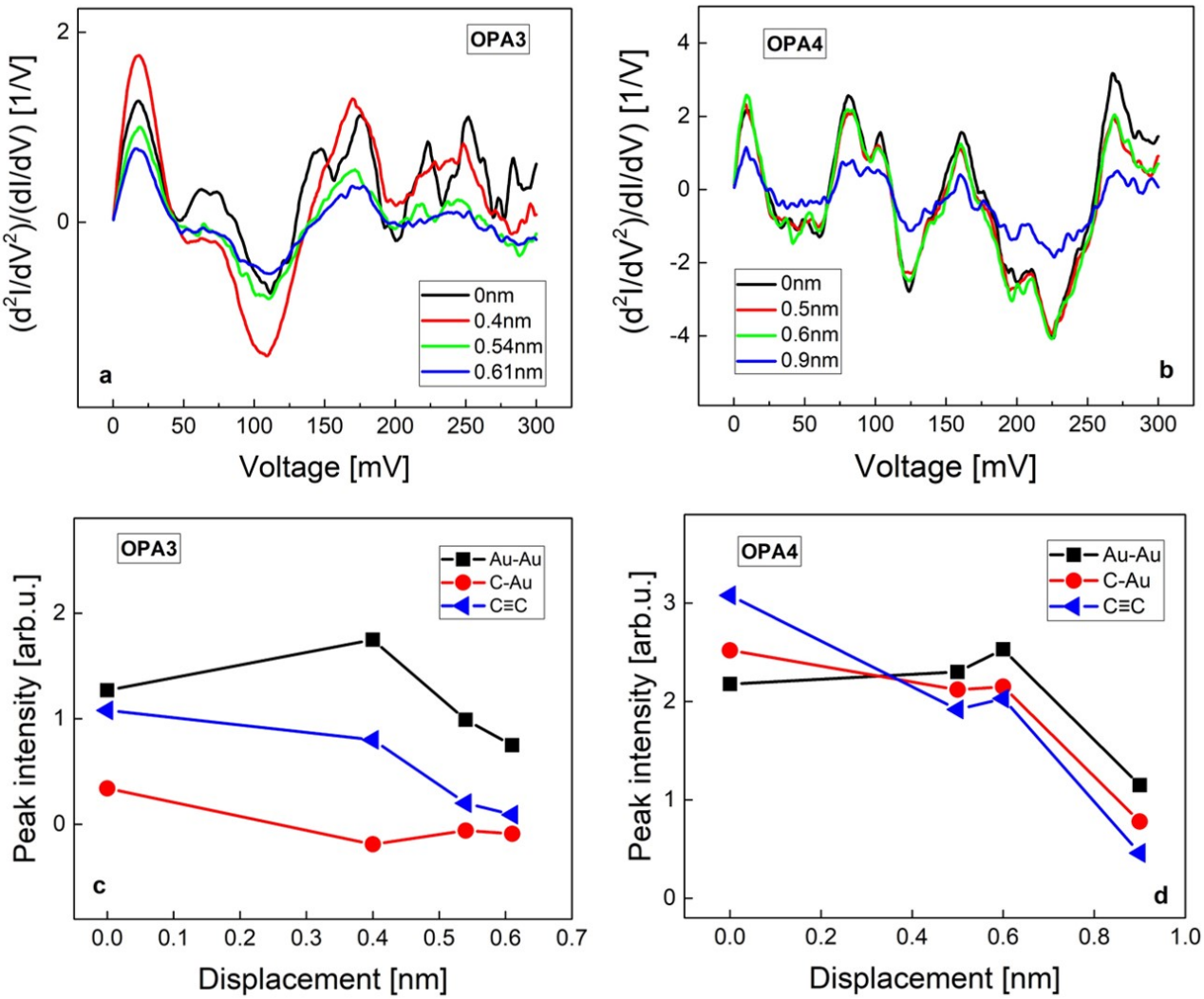

Figure 4: IETS spectra measured for different stretching displacements in the HC regime of OPA3 (a) and OPA4 (b) molecule junctions. Evolution of peak intensities observed for Au - Au, Au - C and C ≡ C vibrational modes from the same contact for OPA3 (c) and OPA4 (d) is also shown.

distinct vibrational C ≡ C modes separated by less than 10 meV. The presence of the C ≡ C-H stretching above 400 meV as shown in Figure S6 would allow to give some hints to this hypothesis but unfortunately this part of the IETS spectrum cannot be accessed experimentally because of stability issues under high bias. Nevertheless, since the IETS were done for the HC regime junctions, the calculated substantial drop in the conductance for single-gold-coordinated systems rule out this possibility.

Reference [21] dealing with ambient condition MCBJs measurements of the OPA_n series suggested the sp_2 - hybridized carbon to explain the unusual ordering in the conductance when increasing the number of phenyl groups as well as the presence of two distinct preferred conductance values. We performed the vibrational study of the arrangement C, D and E to study this possibility (Table 1). The vibrational signature of a C ≡ C around 275 meV disappears and the C=C vibrational modes is much lower in energy, 250 meV in case C down to 220 meV for case D and E (in the same region than the phenyl vibrational region). This result does not satisfactorily explain the IETS measurements. We also investigated the possibility of the presence of a dimer OPA2-OPA2 resulting from C-C coupling. As already mentioned,this reaction was observed experimentally for OPA3 on Ag(111) metallic surfaces.[42] Gold is also

able to induce the same reaction as recently reported for phenylacetylene homocoupling.[41] The $(OPA2)_2$ vibrational signature in the region around 275 meV consists of two distinct peaks separated by 15 meV and is due to the terminal vibrational motion of the C ≡ C and the C ≡ C - C ≡ C central units of the molecule. This could explain the more structured IETS peaks for some of the OPA2 measurements.

To further study the contact geometries and the evolution of these junctions upon stretching, we have compared the IET spectra from the HC regime of OPA3 and OPA4. Figure 4 shows the IET spectra measured for increasing stretching distance starting from the initial formation of an OPA3 and OPA4 molecule junction. We have analyzed the changes in peak intensities of the Au - Au, Au - C and C ≡ C modes upon stretching. For OPA3, the amplitude of the Au - C phonon mode is considerably lower compared to the other modes and to the Au - C mode of the other molecules, (see, Figure S4 in SI for comparison of averaged IETS) which suggests only a weak bond, or a bond on only one side may have formed. Upon stretching the junction, we also found that the amplitudes of the Au - C and C ≡ C modes clearly reduce, supporting this interpretation (Figure 4). In the case of OPA4, the amplitudes of these vibrational modes are observed to be large compared to other phonon modes until around 0.6 nm. The IET spectra tend to be stable with minimal changes of the Au - C mode and a significant change in the C ≡ C mode which corroborates the strong bonding between the Au and the end-standing C atom. A drastic decrease in vibrational excitations after this point is assigned to the rupture of the junction. The stretching distance and stability of IETS aligns with the observed average plateau length in our trace analysis. The initial enhancement of the Au phonon mode upon stretching is attributed to the formation of an atomic chain due to weak bonding strength of Au - Au atoms [39], as also observed in the Au - thiol junctions.[32] These findings further confirm the presence of molecular junctions using Au - C covalent bonding at low temperature. Said that, a detailed future research on the LC regime of these molecules is required to completely understand the nature of bond formation and contact geometries in these systems.

4 Conclusions

To conclude, we have developed single molecular junctions using direct Au - C covalent bonding at low temperature using OPAn chains. We demonstrated the presence of molecular junctions between Au electrodes using conventional conductance histograms revealing several peaks for all molecules corresponding to different binding configurations. The IETS and detailed phonon mode analysis using DFT calculations revealed the presence of the Au - C vibron mode and the C ≡ C bands providing further evidence to our analysis, which suggests that the Au - C linking scheme is suitable for the formation of molecular wires as platform for functional molecular devices, also at low temperature. The study clearly shows that although all three molecules belong to the same class of molecular wires with the same endgroups, the actually formed junctions can be quite different and may have different formation yield. Our analysis also demonstrates the importance of the combination of complementary measurement techniques to elucidate the real nature of molecular junctions.

5 Acknowledgements

We thank M. Hybertsen, A. Erbe, T. Huhn and the members of the SFB767 discussion group for fruitful interaction and A. Fischer, M. Hagner, S. Haus, J. Maier and R. Sieber for technical support. We acknowledge funding by the Deutsche Forschungsgemeinschaft (DFG - German Research Foundation) through SFB767. Also, we gratefully acknowledge the support of the fol-

lowing institutions: the French "Centre National de la Recherche Scientifique" (CNRS), the University of Rennes 1, the National Fund for Scientific Research (FNRS, Belgium). K.C. and V.D. acknowledge support by the "Grand équipement national de calcul intensif (GENCI)" through HPC resources of CINES, IDRIS and TGCC (grants 2020/2021-A0080800649/A0100800649). J.C. is a research director of the Belgian Natioanl Fund for Scientific Research (FNRS).

References

[1] Nitzan, A. Electron Transport in Molecular Wire Junctions. Science (80-.). 2003, 300 (5624), 1384–1389. https://doi.org/10.1126/science.1081572.

[2] Song, H.; Reed, M. A.; Lee, T. Single Molecule Electronic Devices. Adv. Mater. 2011, 23 (14), 1583–1608. https://doi.org/10.1002/adma.201004291.

[3] Kaliginedi, V.; V. Rudnev, A.; Moreno-García, P.; Baghernejad, M.; Huang, C.; Hong, W.; Wandlowski, T. Promising Anchoring Groups for Single-Molecule Conductance Measurements. Phys. Chem. Chem. Phys. 2014, 16 (43), 23529–23539. https://doi.org/10.1039/c4cp03605k.

[4] Hong, W.; Manrique, D. Z.; Moreno-García, P.; Gulcur, M.; Mishchenko, A.; Lambert, C. J.; Bryce, M. R.; Wandlowski, T. Single Molecular Conductance of Tolanes: Experimental and Theoretical Study on the Junction Evolution Dependent on the Anchoring Group. J. Am. Chem. Soc. 2012, 134 (4), 2292–2304. https://doi.org/10.1021/ja209844r.

[5] Chen, F.; Li, X.; Hihath, J.; Huang, Z.; Tao, N. Effect of Anchoring Groups on Single-Molecule Conductance: Comparative Study of Thiol-, Amine-, and Carboxylic-Acid-Terminated Molecules. J. Am. Chem. Soc. 2006, 128 (49), 15874–15881. https://doi.org/10.1021/ja065864k.

[6] Hines, T.; Díez-Pérez, I.; Nakamura, H.; Shimazaki, T.; Asai, Y.; Tao, N. Controlling Formation of Single-Molecule Junctions by Electrochemical Reduction of Diazonium Terminal Groups. J. Am. Chem. Soc. 2013, 135 (9), 3319–3322. https://doi.org/10.1021/ja3106434.

[7] Venkataraman, L.; Klare, J. E.; Tam, I. W.; Nuckolls, C.; Hybertsen, M. S.; Steigerwald, M. L. Single-Molecule Circuits with Well-Defined Molecular Conductance. Nano Lett. 2006, 6 (3), 458–462. https://doi.org/10.1021/nl052373.

[8] Huang, Z.; Chen, F.; Bennett, P. A.; Tao, N. Single Molecule Junctions Formed via Au-Thiol Contact: Stability and Breakdown Mechanism. J. Am. Chem. Soc. 2007, 129 (43), 13225–13231. https://doi.org/10.1021/ja074456t.

[9] Quek, S. Y.; Venkataraman, L.; Choi, H. J.; Louie, S. G.; Hybertsen, M. S.; Neaton, J. B. Amine - Gold Linked Single-Molecule Circuits: Experiment and Theory. Nano Lett. 2007, 7 (11), 3477–3482. https://doi.org/10.1021/nl072058i.

[10] Hybertsen, M. S.; Venkataraman, L.; Klare, J. E.; Whalley, A. C.; Steigerwald, M. L.; Nuckolls, C. Amine-Linked Single-Molecule Circuits: Systematic Trends across Molecular Families. J. Phys. Condens. Matter 2008, 20 (37). https://doi.org/10.1088/0953-8984/20/37/374115.

[11] Zotti, L. A.; Kirchner, T.; Cuevas, J. C.; Pauly, F.; Huhn, T.; Scheer, E.; Erbe, A. Revealing the Role of Anchoring Groups in the Electrical Conduction through Single-Molecule Junctions. Small 2010, 6 (14), 1529–1535. https://doi.org/10.1002/smll.200902227.

[12] Tam, E. S.; Parks, J. J.; Shum, W. W.; Zhong, Y. W.; Santiago-Berríos, M. B.; Zheng, X.; Yang, W.; Chan, G. K. L.; Abruña, H. D.; Ralph, D. C. Single-Molecule Conductance of Pyridine-Terminated Dithienylethene Switch Molecules. ACS Nano 2011, 5 (6), 5115–5123. https://doi.org/10.1021/nn201199b.

[13] Cheng, Z. L.; Skouta, R.; Vazquez, H.; Widawsky, J. R.; Schneebeli, S.; Chen, W.; Hybertsen, M. S.; Breslow, R.; Venkataraman, L. In Situ Formation of Highly Conducting Covalent Au-C Contacts for Single-Molecule Junctions. Nat. Nanotechnol. 2011, 6 (6), 353–357. https://doi.org/10.1038/nnano.2011.66.

[14] Chen, W.; Widawsky, J. R.; Vázquez, H.; Schneebeli, S. T.; Hybertsen, M. S.; Breslow, R.; Venkataraman, L. Highly Conducting π-Conjugated Molecular Junctions Covalently Bonded to Gold Electrodes. J. Am. Chem. Soc. 2011, 133 (43), 17160–17163. https://doi.org/10.1021/ja208020j.

[15] Widawsky, J. R.; Chen, W.; Vázquez, H.; Kim, T.; Breslow, R.; Hybertsen, M. S.; Venkataraman, L. Length-Dependent Thermopower of Highly Conducting Au-C Bonded Single Molecule Junctions. Nano Lett. 2013, 13 (6), 2889–2894. https://doi.org/10.1021/nl4012276.

[16] Pla-Vilanova, P.; Aragonès, A. C.; Ciampi, S.; Sanz, F.; Darwish, N.; Diez-Perez, I. The Spontaneous Formation of Single-Molecule Junctions via Terminal Alkynes. Nanotechnology 2015, 26 (38). https://doi.org/10.1088/0957-4484/26/38/381001.

[17] Ricci, A. M.; Calvo, E. J.; Martin, S.; Nichols, R. J. Electrochemical Scanning Tunneling Spectroscopy of Redox-Active Molecules Bound by Au-C Bonds. J. Am. Chem. Soc. 2010, 132 (8), 2494–2495. https://doi.org/10.1021/ja907867b.

[18] Hong, W.; Li, H.; Liu, S. X.; Fu, Y.; Li, J.; Kaliginedi, V.; Decurtins, S.; Wandlowski, T. Trimethylsilyl-Terminated Oligo(Phenylene Ethynylene)s: An Approach to Single-Molecule Junctions with Covalent Au-C σ-Bonds. J. Am. Chem. Soc. 2012, 134 (47), 19425–19431. https://doi.org/10.1021/ja307544w.

[19] Arasu, N. P.; Vázquez, H. Direct Au-C Contacts Based on Biphenylene for Single Molecule Circuits. Phys. Chem. Chem. Phys. 2018, 20 (15), 10378–10383. https://doi.org/10.1039/c8cp00613j.

[20] Schwarz, F.; Kastlunger, G.; Lissel, F.; Riel, H.; Venkatesan, K.; Berke, H.; Stadler, R.; Lörtscher, E. High-Conductive Organometallic Molecular Wires with Delocalized Electron Systems Strongly Coupled to Metal Electrodes. Nano Lett. 2014, 14 (10), 5932–5940. https://doi.org/10.1021/nl5029045.

[21] Olavarria-Contreras, I. J.; Perrin, M. L.; Chen, Z.; Klyatskaya, S.; Ruben, M.; Van Der Zant, H. S. J. C-Au Covalently Bonded Molecular Junctions Using Non-protected Alkynyl Anchoring Groups. J. Am. Chem. Soc. 2016, 138 (27), 8465–8469. https://doi.org/10.1021/jacs.6b03383.

[22] Batra, A.; Kladnik, G.; Gorjizadeh, N.; Steigerwald, M.; Nuckolls, C.; Quek, S. Y.; Cvetko, D.; Morgante, A.; Venkataraman, L. Trimethyltin-Mediated Covalent Gold-Carbon Bond Formation. 2014. J. Am. Chem. Soc. 2014, 136 (36), 12556–12559. https://doi.org/10.1021/ja5061406

[23] Vrouwe, S. A. G.; Van Der Giessen, E.; Van Der Molen, S. J.; Dulic, D.; Trouwborst, M. L.; Van Wees, B. J. Mechanics of Lithographically Defined Break Junctions. Phys. Rev. B - Condens. Matter Mater. Phys. 2005, 71 (3), 1–7. https://doi.org/10.1103/PhysRevB.71.035313.

[24] Böhler, T.; Edtbauer, A.; Scheer, E. Conductance of Individual C_{60} Molecules Measured with Controllable Gold Electrodes. Phys. Rev. B - Condens. Matter Mater. Phys. 2007, 76 (12), 1–5. https://doi.org/10.1103/PhysRevB.76.125432.

[25] Böhler, T.; Grebing, J.; Mayer-Gindner, A.; Löhneysen, H. V.; Scheer, E. Mechanically Controllable Break-Junctions for Use as Electrodes for Molecular Electronics. Nanotechnology 2004, 15 (7). https://doi.org/10.1088/0957-4484/15/7/054.

[26] Maity, P.; Takano, S.; Yamazoe, S.; Wakabayashi, T.; Tsukuda, T. Binding Motif of Terminal Alkynes on Gold Clusters. J. Am. Chem. Soc. 2013, 135 (25), 9450–9457. https://doi.org/10.1021/ja401798z.

[27] Martín, S.; Grace, I.; Bryce, M. R.; Wang, C.; Jitchati, R.; Batsanov, A. S.; Higgins, S. J.; Lambert, C. J.; Nichols, R. J. Identifying Diversity in Nanoscale Electrical Break Junctions. J. Am. Chem. Soc. 2010, 132 (26), 9157–9164. https://doi.org/10.1021/ja103327f.

[28] Quek, S. Y.; Choi, H. J.; Louie, S. G.; Neaton, J. B. Length Dependence of Conductance in Aromatic Single-Molecule Junctions. Nano Lett. 2009, 9 (11), 3949–3953. https://doi.org/10.1021/nl9021336.

[29] Foti, G.; Vázquez, H.; Sánchez-Portal, D.; Arnau, A.; Frederiksen, T. Identifying Highly Conducting Au-C Links through Inelastic Electron Tunneling Spectroscopy. J. Phys. Chem. C 2014, 118 (46), 27106–27112. https://doi.org/10.1021/jp5077824.

[30] Frederiksen, T.; Paulsson, M.; Brandbyge, M.; Jauho, A. P. Inelastic Transport Theory from First Principles: Methodology and Application to Nanoscale Devices. Phys. Rev. B - Condens. Matter Mater. Phys. 2007, 75 (20), 1–22. https://doi.org/10.1103/PhysRevB.75.205413.

[31] Arroyo, C. R.; Frederiksen, T.; Rubio-Bollinger, G.; Vélez, M.; Arnau, A.; Sánchez-Portal, D.; Agraït, N. Characterization of Single-Molecule Pentanedithiol Junctions by Inelastic Electron Tunneling Spectroscopy and First-Principles Calculations. Phys. Rev. B - Condens. Matter Mater. Phys. 2010, 81 (7), 4–8. https://doi.org/10.1103/PhysRevB.81.075405.

[32] Kim, Y.; Song, H.; Strigl, F.; Pernau, H. F.; Lee, T.; Scheer, E. Conductance and Vibrational States of Single-Molecule Junctions Controlled by Mechanical Stretching and Material Variation. Phys. Rev. Lett. 2011, 106 (19), 2–5. https://doi.org/10.1103/PhysRevLett.106.196804.

[33] Fu, T.; Smith, S.; Camarasa-Gómez, M.; Yu, X.; Xue, J.; Nuckolls, C.; Evers, F.; Venkataraman, L.; Wei, S. Enhanced Coupling through π-Stacking in Imidazole-Based Molecular Junctions. Chem. Sci. 2019, 10 (43), 9998–10002. https://doi.org/10.1039/c9sc03760h.

[34] Kula, M.; Jiang, J.; Luo, Y. Probing Molecule-Metal Bonding in Molecular Junctions by Inelastic Electron Tunneling Spectroscopy. Nano Lett. 2006, 6 (8), 1693–1698. https://doi.org/10.1021/nl060951w.

[35] Paulsson, M.; Frederiksen, T.; Brandbyge, M. Inelastic Transport through Molecules: Comparing First-Principles Calculations to Experiments. Nano Lett. 2006, 6 (2), 258–262. https://doi.org/10.1021/nl052224r.

[36] Kushmerick, J. G.; Lazorcik, J.; Patterson, C. H.; Shashidnar, R.; Seferos, D. S.; Bazan, G. C. Vibronic Contributions to Charge Transport across Molecular Junctions. Nano Lett. 2004, 4 (4), 639–642. https://doi.org/10.1021/nl049871n.

[37] Kim, Y.; Hellmuth, T. J.; Bürkle, M.; Pauly, F.; Scheer, E. Characteristics of Amine-Ended and Thiol-Ended Alkane Single-Molecule Junctions Revealed by Inelastic Electron Tunneling Spectroscopy. ACS Nano 2011, 5 (5), 4104–4111. https://doi.org/10.1021/nn200759s.

[38] Laurentius, L.; Stoyanov, S. R.; Gusarov, S.; Kovalenko, A.; Du, R.; Lopinski, G. P.; McDermott, M. T. Diazonium-Derived Aryl Films on Gold Nanoparticles: Evidence for a Carbon-Gold Covalent Bond. ACS Nano 2011, 5 (5), 4219–4227. https://doi.org/10.1021/nn201110r.

[39] Agraït, N.; Untiedt, C.; Rubio-Bollinger, G.; Vieira, S. Onset of Energy Dissipation in Ballistic Atomic Wires. Phys. Rev. Lett. 2002, 88 (21), 4. https://doi.org/10.1103/PhysRevLett.88.216803.

[40] Kanuru, V. K.; Kyriakou, G.; Beaumont, S. K.; Papageorgiou, A. C.; Watson, D. J.; Lambert, R. M. Sonogashira Coupling on an Extended Gold Surface in Vacuo: Reaction of Phenylacetylene with Iodobenzene on Au(111). J. Am. Chem. Soc. 2010, 132 (23), 8081–8086. https://doi.org/10.1021/ja1011542.

[41] Sánchez-Sánchez, C.; Yubero, F.; González-Elipe, A. R.; Feria, L.; Sanz, J. F.; Lambert, R. M. The Flexible Surface Revisited: Adsorbate-Induced Reconstruction, Homocoupling, and Sonogashira Cross-Coupling on the Au(100) Surface. J. Phys. Chem. C 2014, 118 (22), 11677–11684. https://doi.org/10.1021/jp501321u.

[42] Sanchez-Sanchez, C.; Orozco, N.; Holgado, J. P.; Beaumont, S. K.; Kyriakou, G.; Watson, D. J.; Gonzalez-Elipe, A. R.; Feria, L.; Fernández Sanz, J.; Lambert, R. M. Sonogashira Cross-Coupling and Homocoupling on a Silver Surface: Chlorobenzene and Phenylacetylene on Ag(100). J. Am. Chem. Soc. 2015, 137 (2), 940–947. https://doi.org/10.1021/ja5115584.

[43] Liu, L.; Liu, Z.; Xu, W.; Xu, H.; Zhang, D.; Zhu, D. Syntheses, Optical and Electrochemical Properties of 4,4'-Bis-[2-(3,4-Dibutyl-2-Thienylethynyl)] Biphenyl and Its Oligomers. Tetrahedron 2005, 61 (15), 3813–3817. https://doi.org/10.1016/j.tet.2005.01.133.

[44] Cirera, B.; Zhang, Y. Q.; Björk, J.; Klyatskaya, S.; Chen, Z.; Ruben, M.; Barth, J. V.; Klappenberger, F. Synthesis of Extended Graphdiyne Wires by Vicinal Surface Templating. Nano Lett. 2014, 14 (4), 1891–1897. https://doi.org/10.1021/nl4046747.

[45] Mohammadparast, F.; Dadgar, A. P.; Tirumala, R. T. A.; Mohammad, S.; Topal, C. O.; Kalkan, A. K.; Andiappan, M. C-C Coupling Reactions Catalyzed by Gold Nanoparticles: Evidence for Substrate-Mediated Leaching of Surface Atoms Using Localized Surface Plasmon Resonance Spectroscopy. J. Phys. Chem. C 2019, 123 (18), 11539–11545. https://doi.org/10.1021/acs.jpcc.8b12453.

Supplementary Information

1 Device Fabrication

The samples were fabricated on a mechanically polished bronze wafer of approximately 250μm thickness, spin coated with polyimide ($\approx 2\mu$m) which acts as an electrical insulator and as a sacrificial layer. The coated wafer is baked at 130° C for 30 min and vacuum annealed at 430° C for 90 min. A double layer of electron beam resists MMA-MAA/PMMA is deposited on top of these wafers and hard baked in an oven at 170° C for 30 min. The wafer is cut into 3 $\times$ 18mm^2 pieces and electron beam lithography is performed. The wafers are developed using 1:3 MIBK:IPA solution for 30s. The developed samples are covered with 80nm of Au using electron beam evaporation. Finally before depositing the molecules, these samples were etched using reactive ion etching in oxygen plasma at 1 hPa and 35W for 30 min. This will develop a free-standing bridge after removing about 600nm of polyimide.

2 Molecule Deposition

Molecule solutions were made using dichloromethane (DCM). OPAn solutions were made with upto 5 mM concentration of OPA2, OPA3 and OPA4 synthetized as previously reported.[21] These are dropcasted onto the freshly etched substrate under nitrogen atmosphere at room temperature. For each experiment we used freshly prepared molecular solutions to avoid any contamination or decomposition.

3 Low-Temperature Transport Measurements

Low-temperature transport measurements were carried out using a custom made cryogenic vacuum dipstick with a MCBJ. After drying the samples properly, they are mounted on the break junction mechanism which is controlled using a dc motor. The wiring is composed of homemade coaxial cables and SMA connectors to avoid any electronic noise. The sample under test is protected using a copper shield to avoid effects of electromagnetic fields. All the measurements are carried out under vacuum and at 4.2 K inside a liquid-He dewar. For the transport measurements, we have used a programmable dc source (Yokogawa 7651), low noise current and voltage amplifiers (Femto DLCPA and Femto DLPVA respectively), Agilent 34410A multimeters and HF2LI lock-in amplifier from Zurich instruments. A sinusoidal AC signal of 3 mV at 713 Hz is combined with the DC voltage using a homemade summation amplifier and is fed to the sample. Grounding of the measurement units is carefully designed to avoid any sort of ground loops and additional noise contribution. The IETS signal is obtained using the simultaneous measurement of first and second harmonic signal from lock-in amplifier. All measurement devices including the motor are remotely controlled using a homemade python based controlling software.

4 Concentration Dependence of Molecule Junction Formation

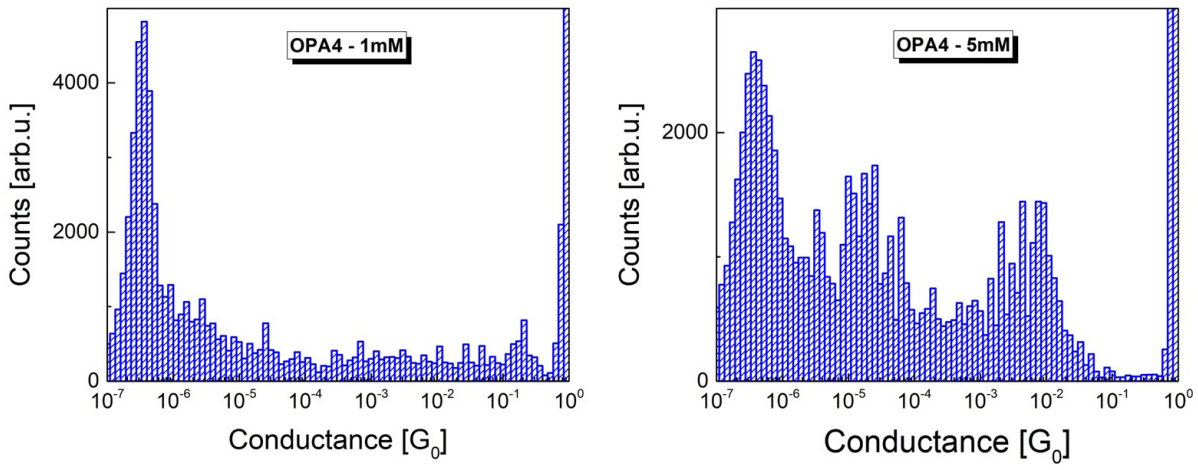

Figure S1: Low-temperature 1D conductance histograms constructed for OPA4 molecules measured by dropcasting 1 mM and 5 mM solutions at 100 mV bias.

5 Probability of Types of Molecular Traces from OPA4

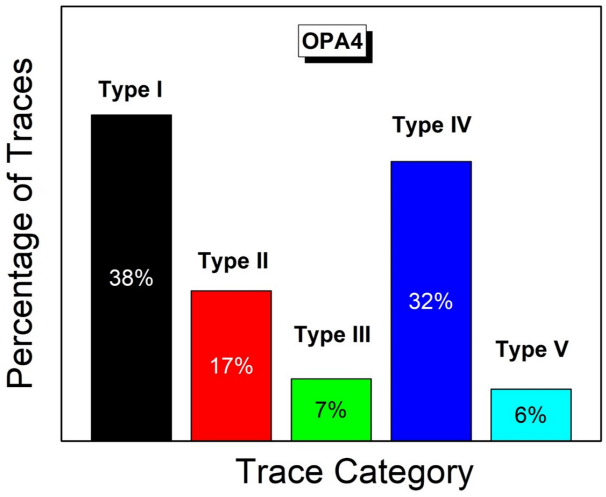

Figure S2: Percentage of molecular traces obtained from OPA4 samples corresponding to each trace category, see main text for more details.

6 Comparison of Lock-in and Numerically Calculated IETS

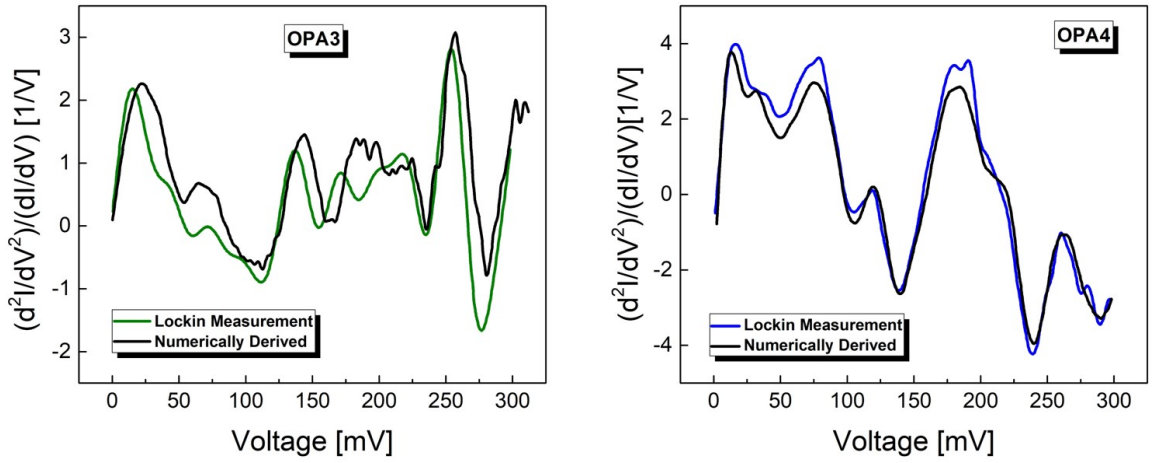

Figure S3: Comparison of inelastic electron tunneling spectra from direct lock-in measurements and numerically derived from dI/dV shown for OPA3 (left) and OPA4 (right).

7 Averaged IET spectra

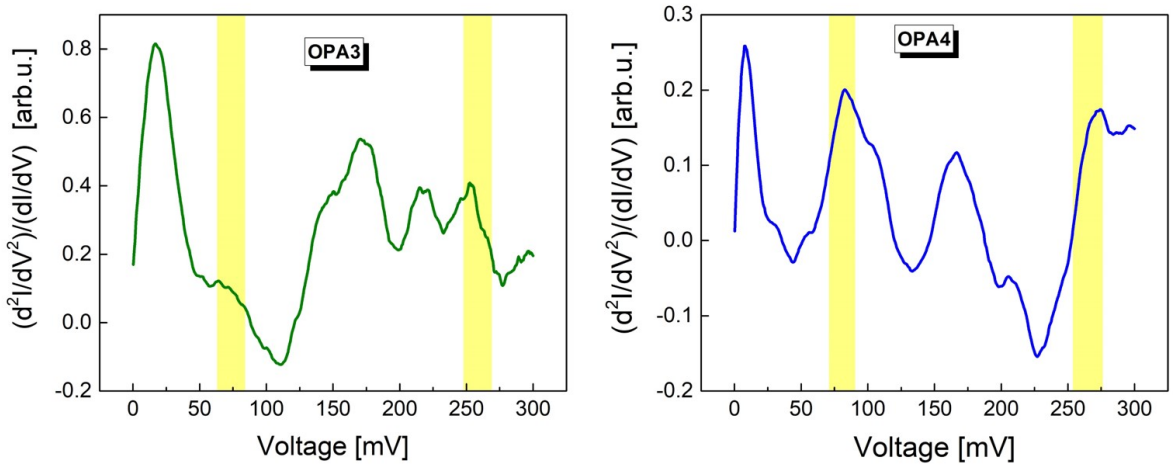

Figure S4: Inelastic electron tunneling spectra for OPA3 and OPA4 after averaging over 10 individual contacts. The yellow regions indicate the typical energies of Au - C vibrons (60 - 75 mV) and of the C ≡ C stretching mode (250 - 275 mV).

8 Computational Details

Molecular geometry optimizations of the OPA systems were performed applying the density functional theory method (DFT with the revPBE functional using a Slater TZ2P atomic basis set with a small frozen core), as implemented in the SCM ADF suite of the program.[1] The Cartesian coordinates of the optimized structures are given in Table S2, S3 and S4 for OPA2, OPA3 and OPA4 respectively. Analytical vibrational frequency calculations were performed, including the calculation of the infrared and Raman intensities; the calculated frequencies ensure that all geometries are minimum on the potential energy surface. The densities of vibrational states were also plotted by using a Gaussian broadening for each vibrational state (with a FWHM = 3 meV).

The simulation of the vibrational properties of the Au - Molecule - Au junctions and monocoordinated Au - molecule systems were simulated by an Au_3 cluster model using the self-consistent-charge density functional tight-binding method (SCC-DFTB2) using the DFTB+, 20.1 code.[2] Additional calculations showed no sensible changes in the vibrational property results when increasing the cluster size up to Au_{13}. The parameter sets "mio" and "auorg" were used. The geometry optimizations were converged imposing a force criterion of 1.10^{-5} a.u. In all cases, no imaginary frequencies were found ensuring that all geometries correspond to a minimum of the potential energy surface (MODES procedure). The densities of vibrational states were obtained by using a Gaussian broadening for each vibrational state (FWHM = 3 meV).

The calculations of the transport properties of the molecular junctions were performed by employing the DFT and the non-equilibrium Green's function (NEGF) approach, as implemented in the QuantumWise ATK 2020 package.[3] The geometries obtained for the isolated molecules were used to build the molecular devices. The distance between the terminal carbon and the flat gold surface was set at 1.97 Å in a top position (optimized distance obtained with the DFTB calculations with the model cluster). The semi-infinite gold electrodes were cleaved in the (111) direction as represented in Figure S7. Ghost atoms were added near the gold surface to reproduce the experimental work function of Au. The ATK computational details used are: GGA RevPBE exchange-correlation functional; FHI (Trouiller–Martins type) atomic basis set double-zeta plus polarization for C and H and single-zeta polarized basis for Au; SCF accuracy tolerance of 1.10^{-5} Hartree; Density mesh cut-off 100 Hartree; $5 \times 5 \times 75$ k-points (along the a, b, and c directions, with c the transport direction) using the Monkhorst-Pack grid; Weighted semi-circle method with integral lower bound of 50 eV and 50 circle points; Fast Fourier transform 2D Poisson solver.

Zero-bias transmission spectra were simulated by calculating 801 points between -2.0 eV and 2.0 eV (Fermi energy located at 0.0 eV), with 5 x 5 k-points in the a and b direction.

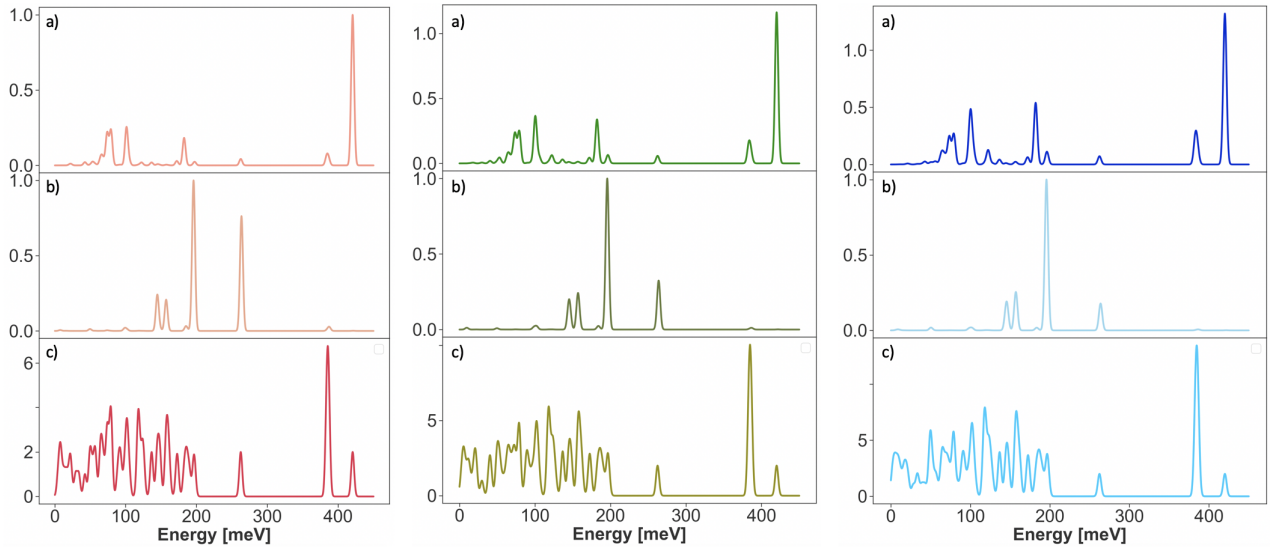

Figure S5: Vibrational study for the bare OPA2 (left), OPA3 (middle) and OPA4 (right) molecule at the DFT level. The Gaussian smearing is set to $\sigma = 3$ meV. a) Calculated IR intensity normalized in arbitrary units. b) Calculated Raman intensity normalized in arbitrary units. c) Calculated vibrational density of modes in eV^{-1}. The carbon triple bond carbon is situated at 265 meV for OPA2, OPA3 and OPA4.

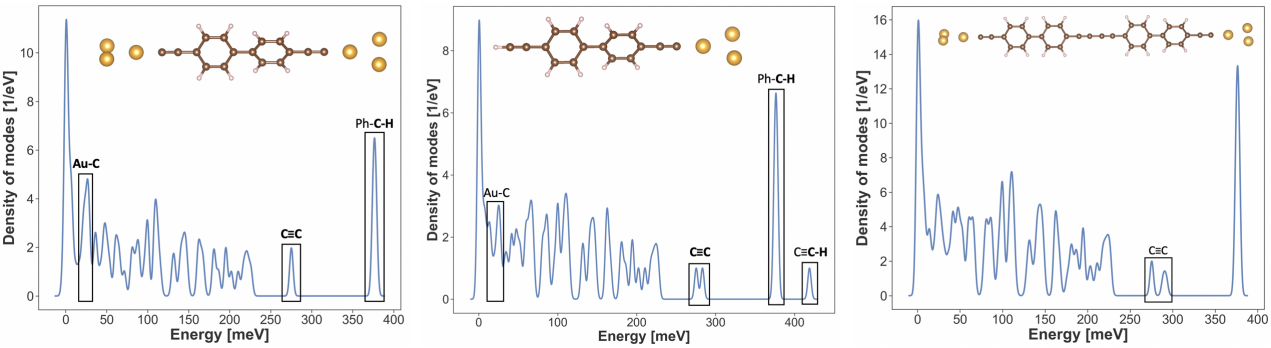

Figure S6: DFTB vibrational density of states of OPA2-A (left), OPA2-B (middle) and (OPA2)2-A (right).

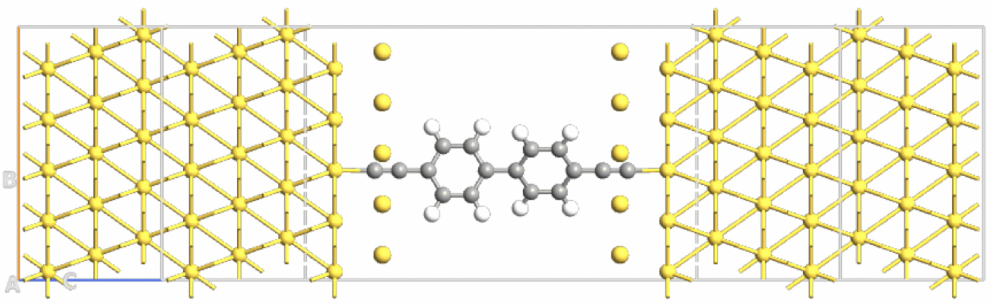

Figure S7: Representation of the OPA2 molecular device, as simulated in Quantum ATK 2020. The yellow spheres above the surfaces represent the ghost atoms.

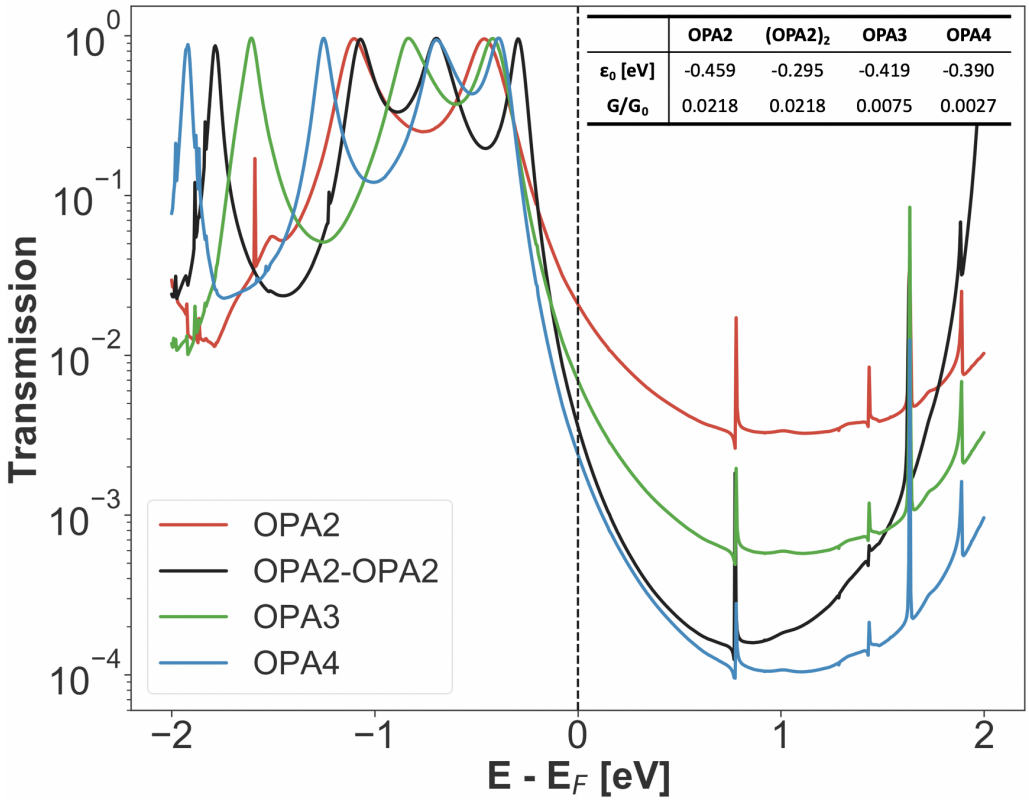

Figure S8: Transmission spectrum of OPA2, OPA2-OPA2, OPA3 and OPA4 at zero bias. ϵ_0 given in eV is the energetic position of the main peak responsible for the conductance of the system with respect to the Fermi energy, G/G_0 is the conductance. The spikes present after the Fermi level are artefacts between the gold interface and the molecule.

9 Cartesian coordinates of the optimized OPA2, OPA3 and OPA4 molecules at the DFT level with ADF:

Table S1: Cartesian coordinates of the OPA2 molecule

C	-2.736816	0.216343	0.146977
C	-1.350821	0.344213	0.202030
C	-3.551734	1.330774	-0.154017
C	-0.717551	1.582542	-0.036322
C	-2.923717	2.573615	-0.393940
C	-1.537140	2.692191	-0.333466
H	-0.748544	-0.527121	0.462770
C	-4.971862	1.204275	-0.214691
H	-3.536498	3.441617	-0.638311
H	3.203658	3.885313	1.062565
H	-1.078344	3.657910	-0.549895
C	2.990833	0.808090	-0.401767
C	3.594361	1.963208	0.144101
C	1.603964	0.689848	-0.456799
C	2.754959	2.991634	0.628276
C	0.760212	1.713456	0.024493
C	1.369144	2.865551	0.565853
C	5.014584	2.088236	0.205852
H	1.165900	-0.201791	-0.907309
H	0.746018	3.663672	0.971628
H	-3.205283	-0.747622	0.346889
H	3.623388	0.009792	-0.790650
C	6.223939	2.195117	0.260491
C	-6.181173	1.096333	-0.268201
H	7.288510	2.289255	0.308152
H	-7.245705	1.001242	-0.314844

Table S2: Cartesian coordinates of the OPA3 molecule

C	-2.919074	0.135028	-0.138792
C	-1.532041	0.249686	-0.080119
C	-3.737614	1.286836	-0.145082
C	-0.900436	1.510355	-0.023881
C	-3.111669	2.552366	-0.087871
C	-1.723856	2.656402	-0.027788
H	-0.926516	-0.657221	-0.049739
C	-5.158827	1.174629	-0.208332
H	-3.727330	3.452109	-0.102057
H	7.390777	4.327627	0.358577
H	-1.267251	3.647015	-0.012373
C	7.116879	0.925344	0.276410
C	7.742803	2.190882	0.333703
C	5.729067	0.821288	0.216314
C	6.924252	3.342682	0.327281
C	4.905641	1.967328	0.212364
C	5.537222	3.228008	0.268582
C	9.164019	2.303110	0.396858
H	5.272461	-0.169325	0.200909
H	4.931676	4.134898	0.238174
H	-3.385606	-0.849911	-0.170142
H	7.732556	0.025613	0.290588
C	10.37427	2.398982	0.452619
C	-6.369079	1.078771	-0.264180
H	11.43958	2.483404	0.501282
H	-7.434386	0.994361	-0.312917
H	3.040181	3.483833	1.523852
C	2.801294	0.858668	-0.631203
C	3.426468	1.850822	0.151990
C	1.412129	0.749362	-0.687586
C	2.593075	2.728290	0.876095
C	0.578735	1.626850	0.036497
C	1.203911	2.618979	0.819716
H	0.965030	-0.006195	-1.335332
H	0.593711	3.291394	1.424592
H	3.411503	0.186239	-1.236054

Table S3: Cartesian coordinates of the OPA4 molecule

C	-2.924252	0.188130	0.277457
C	-1.536088	0.293188	0.327933
C	-3.715661	1.285955	-0.128819
C	-0.876622	1.491219	-0.020069
C	-3.061652	2.488891	-0.477888
C	-1.673016	2.584850	-0.421436
H	-0.952063	-0.562273	0.670220
C	-5.137846	1.182590	-0.186241
H	-3.655988	3.343009	-0.803536
H	11.75268	4.384631	1.251059
H	-1.193820	3.517538	-0.722419
C	11.47802	1.210501	0.023643
C	12.10480	2.386851	0.492653
C	10.08904	1.120555	-0.035198
C	11.28591	3.464813	0.897740
C	9.265378	2.192294	0.370260
C	9.897884	3.364379	0.836532
C	13.52717	2.483995	0.556126
H	9.632502	0.190026	-0.375502
H	9.291156	4.221770	1.131233
H	-3.412753	-0.744120	0.562130
H	12.09417	0.365047	-0.283563
C	14.73842	2.566916	0.612162
C	-6.348971	1.094754	-0.237356
H	15.80458	2.639752	0.661180
H	-7.415015	1.017533	-0.282037
H	3.084238	3.802849	0.871629
C	2.818615	0.620292	-0.308302
C	3.453712	1.796439	0.140329
C	1.428188	0.521411	-0.357446
C	2.629168	2.870382	0.533990
C	0.603853	1.596267	0.034229
C	1.238708	2.774060	0.478956
H	0.973640	-0.400287	-0.724000
H	0.634026	3.621621	0.805424
H	3.423361	-0.237555	-0.606571
H	7.437851	3.146068	2.171814
C	7.137747	1.426513	-0.751455
C	7.784894	2.091213	0.310487
C	5.747162	1.332472	-0.806606
C	6.972427	2.657260	1.314568
C	4.934651	1.898249	0.197593
C	5.581968	2.562932	1.259381
H	5.281389	0.843924	-1.663841
H	4.988602	2.980106	2.074473
H	7.730787	1.009904	-1.567086

References

[1] ADF 2019, SCM, Theoretical Chemistry, Vrije Universiteit, Amsterdam, The Netherlands, http://www.scm.com.

[2] a) M. Elstner, D. Porezag, G. Jungnickel, J. Elsner, M. Haugk, T. Frauenheim, S. Suhai, G. Seifert, Self-consistent-charge density-functional tight-binding method for simulations of complex materials properties, Phys. Rev. B 58 (1998) 7260–7268, https://doi.org/10.1103/PhysRevB.58.7260. b) B. Hourahine, B. Aradi, V. Blum, F. Bonaf e, A. Buccheri, C. Camacho, C. Cevallos, M.Y. Deshaye, T. Dumitrică, A. Dominguez, S. Ehlert, M. Elstner, T. van der Heide, J. Hermann, S. Irle, J.J. Kranz, C. Köhler, T. Kowalczyk, T. Kubăr, I.S. Lee, V. Lutsker, R.J. Maurer, S.K. Min, I. Mitchell, C. Negre, T.A. Niehaus, A.M., N. Niklasson, A.J. Page, A. Pecchia, G. Penazzi, M.P. Persson, J. Řezáč, C. G. Sanchez, M. Sternberg, M. Stohr, F. Stuckenberg, A. Tkatchenko, V.W.-Z. Yu, T. Frauenheim, DFTB+, a software package for efficient approximate density functional theory based atomistic simulations, J. Chem. Phys., 152, 2020,p. 124101, https://doi.org/10.1063/1.5143190.

[3] QuantumATK Q-2020 Synopsys. https://www.synopsys. com/silicon/quantumatk.html.